



# Cu<sub>2</sub>ZnSnS<sub>4</sub>/N-MWCNTs hybrid systems as counter electrode substitutes for platinum in dye-sensitized solar cells

Lineo Mxakaza<sup>1,2</sup>, Grace Ngubeni<sup>1</sup>, Nosipho Moloto<sup>1,a)</sup> , Zikhona Tetana<sup>1,2,a)</sup>

<sup>1</sup>Molecular Sciences Institute, School of Chemistry, University of the Witwatersrand, Private Bag 3, Wits 2050, Johannesburg, South Africa

<sup>2</sup>DSI/NRF Centre of Excellence in Strong Materials, University of the Witwatersrand, Private Bag 3, Wits 2050, Johannesburg, South Africa

<sup>a)</sup>Address all correspondence to these authors. e-mails: Nosipho.Moloto@wits.ac.za; Zikhona.Tetana@wits.ac.za

Received: 21 February 2023; accepted: 1 December 2023; published online: 3 January 2024

Copper zinc tin sulfide, Cu<sub>2</sub>ZnSnS<sub>4</sub> (CZTS) is being considered a viable option for a counter electrode due to its abundance, cost-effectiveness, catalytic activity, and other advantageous properties. However, CZTS has low electron transport capabilities, a shortcoming that can be addressed by combining it with high electron mobility carbon nanomaterials. Nitrogen-doped multi-walled carbon nanotubes (N-MWCNTs) exhibit higher electron conductivities than their pristine counterparts. This improvement is attributed to the disruption of the sp<sup>2</sup>-hybridized carbon arrangement, as some of the carbon atoms are replaced by nitrogen atoms. In this study, a counter electrode composed of a 70% CZTS and 30% N-MWCNTs mixture produced a higher electrochemical current density compared to the individual materials. This suggests that it is more electrocatalytic than CZTS and N-MWCNTs alone, ultimately leading to the highest power conversion efficiency of 6.52%.

## Introduction

Dye-sensitized solar cells (DSSCs), also known as Grätzel cells are rapidly gaining momentum. These cells utilize relatively simple manufacturing technologies, offer promising efficiency, and have low cost of fabrication [1]. However, their commercialization has been hindered by the use of Pt as a counter electrode (CE), among other factors. The noble Pt counter electrode can thus be replaced with more abundant, yet environmentally friendly materials that exhibit similar properties. While Pt demonstrates good catalytic activity toward the common I<sup>-</sup>/I<sub>3</sub><sup>-</sup> DSSCs electrolyte, it is not without its drawbacks; Pt undergoes oxidation to PtI<sub>4</sub> upon prolonged exposure to I<sup>-</sup>/I<sub>3</sub><sup>-</sup> [2, 3].

Transition metal sulfides such as WS<sub>2</sub>, CoS, and NiS have been studied as alternative CE materials [4–6]. However, their catalytic properties do not surpass those of Pt, mainly due to their relatively low conductivities. Chalcogenides, particularly Cu<sub>2</sub>ZnSnS<sub>4</sub> (CZTS), consist of earth-abundant, relatively inexpensive constituent elements, easily optimized synthesis methods, and exhibit decent electrocatalytic activity [7–9]. Nonetheless, a study conducted by Nemala et al. obtained only a 4.5% power conversion efficiency (PCE) when CZTS was employed

as a counter electrode, primarily attributed to its limited conductivity [10]. To address the poor conductivity of CZTS and the subpar catalytic behavior of N-MWCNTs (nitrogen-doped multi-walled carbon nanotubes), a CZTS/MWCNT hybrid can be employed as a counter electrode to enhance catalytic activity and electron transfer in DSSCs [10, 11].

Multi-walled carbon nanotubes (MWCNTs) are cylindrical structures composed of stacked graphene sheets that exhibit stability at high temperatures, elasticity, and conductivity [12]. However, their electrical conductivity can be further enhanced by disrupting the hybridization of sp<sup>2</sup> carbon atoms in the graphitic structure. This is achieved through doping with atoms such as nitrogen to create nitrogen-doped multi-walled carbon nanotubes (N-MWCNTs) [13, 14].

Various hybrid systems combining carbon nanotubes and inorganic nanoparticles have been developed and applied in photovoltaic and energy storage devices, catalysis, and antimicrobial applications [15–18]. Typically, inorganic nanoparticles are dispersed on the surface of the nanotubes, a process that can be accomplished using either in-situ or ex-situ preparation methods.

CNT-chalcogenide hybrid systems have been employed as counter electrodes in dye-sensitized solar cells (DSSCs), where the increased surface area and electron conductivity resulting from the presence of carbon nanotubes enhance the catalytic activity of the counter electrode toward the electrolyte [10]. In this study, we evaluate the performance of CZTS/N-MWCNTs as an efficient alternative counter electrode to Pt for the first time. This evaluation is conducted through cyclic voltammetry studies carried out in a DSSC electrolyte.

## Results and discussion

The X-ray diffraction (XRD) pattern [Fig. 1(a)] of CZTS reveals three prominent peaks at  $2\theta = 28^\circ$ ,  $47^\circ$ , and  $56^\circ$ , corresponding to the [112], [220], and [312] crystal planes, respectively. These peaks are characteristic of CZTS and are consistent with

the kesterite CZTS phase (JCPDS no. 01-075-4122). Upon mixing CZTS with N-MWCNTs, an additional peak is observed at  $28^\circ$  [002], attributed to the presence of carbon material (N-MWCNTs) within the sample matrix. Notably, the intensity of the carbon peak does not exhibit a consistent trend as the concentration of carbon nanotubes increases from 10 to 30 wt %. This variation may be attributed to the uneven distribution of the nanotubes within the CZTS sample. In the XRD pattern of the composites, two small peaks also appear between  $30^\circ$  and  $35^\circ$ , and these are attributed to the presence of metal oxides. Raman spectra of the prepared CZTS, N-MWCNTs, and CZTS/N-MWCNTs are presented in Fig. 1(b)–(d), respectively. The spectrum of CZTS displays two prominent peaks at  $316$  and  $1573$   $\text{cm}^{-1}$ , corresponding to kesterite CZTS and the organic ligand (OLA) attached to the CZTS nanoparticles. The peak at  $316$   $\text{cm}^{-1}$  arises from sulfur vibrations in the crystal

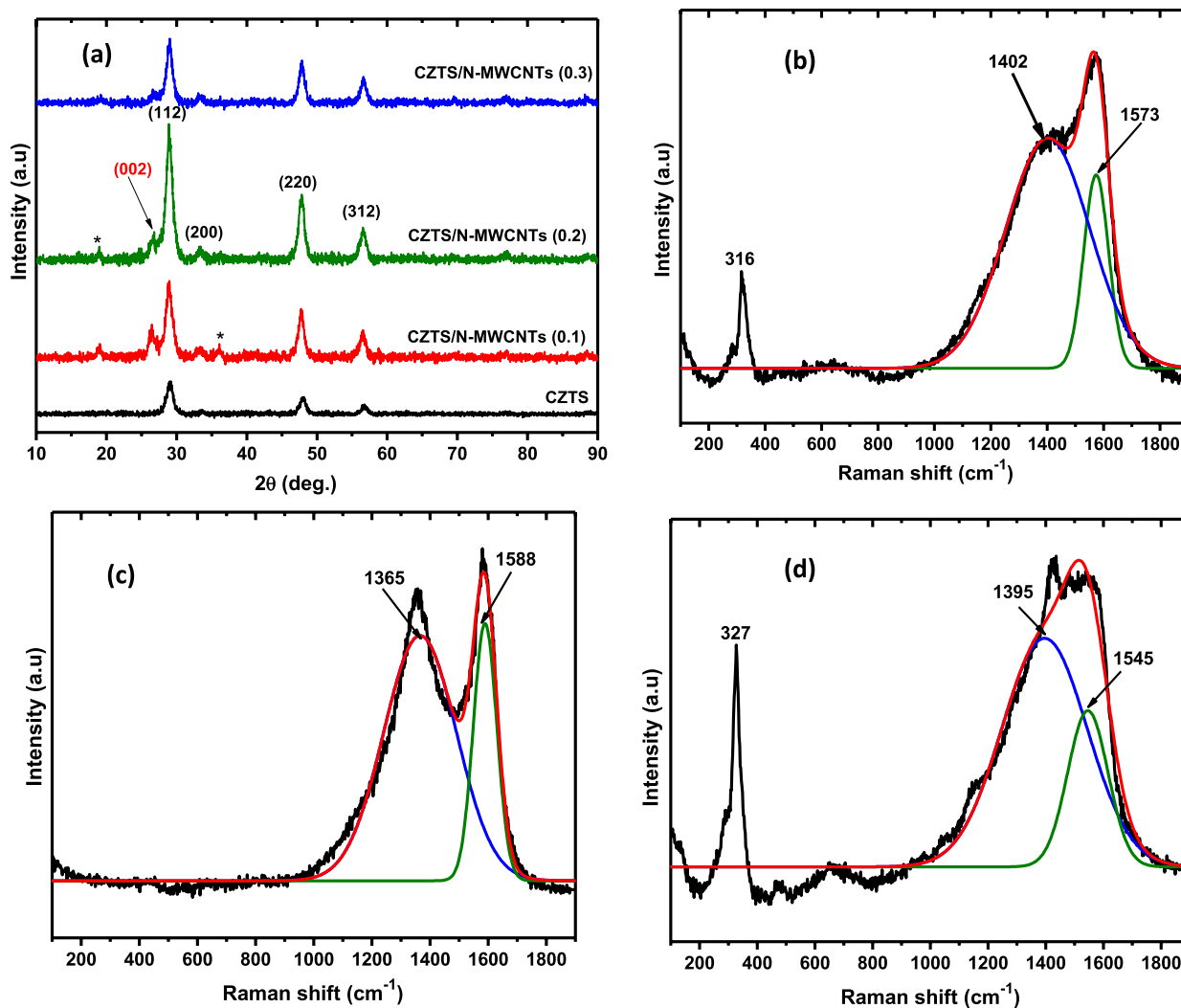


**Figure 1:** (a) XRD pattern of CZTS and CZTS/N-MWCNTs with increasing N-MWCNT concentration (\*denotes metal oxides peaks and (002) is attributed to N-MWCNTs). Raman spectra of (b) CZTS, (c) N-MWCNTs, and (d) CZTS/N-MWCNTs(0.2) nanocomposite.

structure of CZTS, while the other peaks at 1402 and 1573  $\text{cm}^{-1}$  are attributed to OLA, which serves as the capping agent used in the CZTS synthesis process [19].

In comparison to the Raman spectrum of CZTS/N-MWCNTs, the CZTS peak is observed at a higher wavenumber of 327  $\text{cm}^{-1}$ . This shift confirms the existence of an interaction between the nanoparticles and carbon nanotubes, causing an increase in the energy of sulfur vibration. The Raman spectrum of N-MWCNTs exhibits two prominent peaks at 1365  $\text{cm}^{-1}$  (D-band), attributed to flaws in the graphene sheet within the carbon structure, and around 1588  $\text{cm}^{-1}$  (G-band), associated with carbon-carbon bond stretches. The shift in the G-band peak position or the change in peak width can help determine whether the CZTS nanoparticles interact with the walls of the carbon nanotubes in the N-MWCNTs [20].

The observed shift in the G-band peak to a lower wavenumber of 1545  $\text{cm}^{-1}$  in the composite material suggests a decrease in the energy of vibration of the carbon-carbon bond due to the interaction between the nanotube walls and the CZTS nanoparticles [21]. Determining the formation of a nanocomposite is crucial in this study because our goal is to combine the catalytic properties of CZTS with the high electron conductivity of N-MWCNTs. This combination can only be achieved if a nanocomposite is indeed formed.

TEM images of the prepared nanocomposites are presented in Fig. 2(b), (c). In these images, it is evident that the carbon nanotubes exhibit varying diameters, open ends, and are entangled. Meanwhile, the CZTS nanoparticles appear as spherical, polydisperse particles, agglomerated, and unevenly distributed on the surfaces of the carbon nanotubes. Notably, the presence

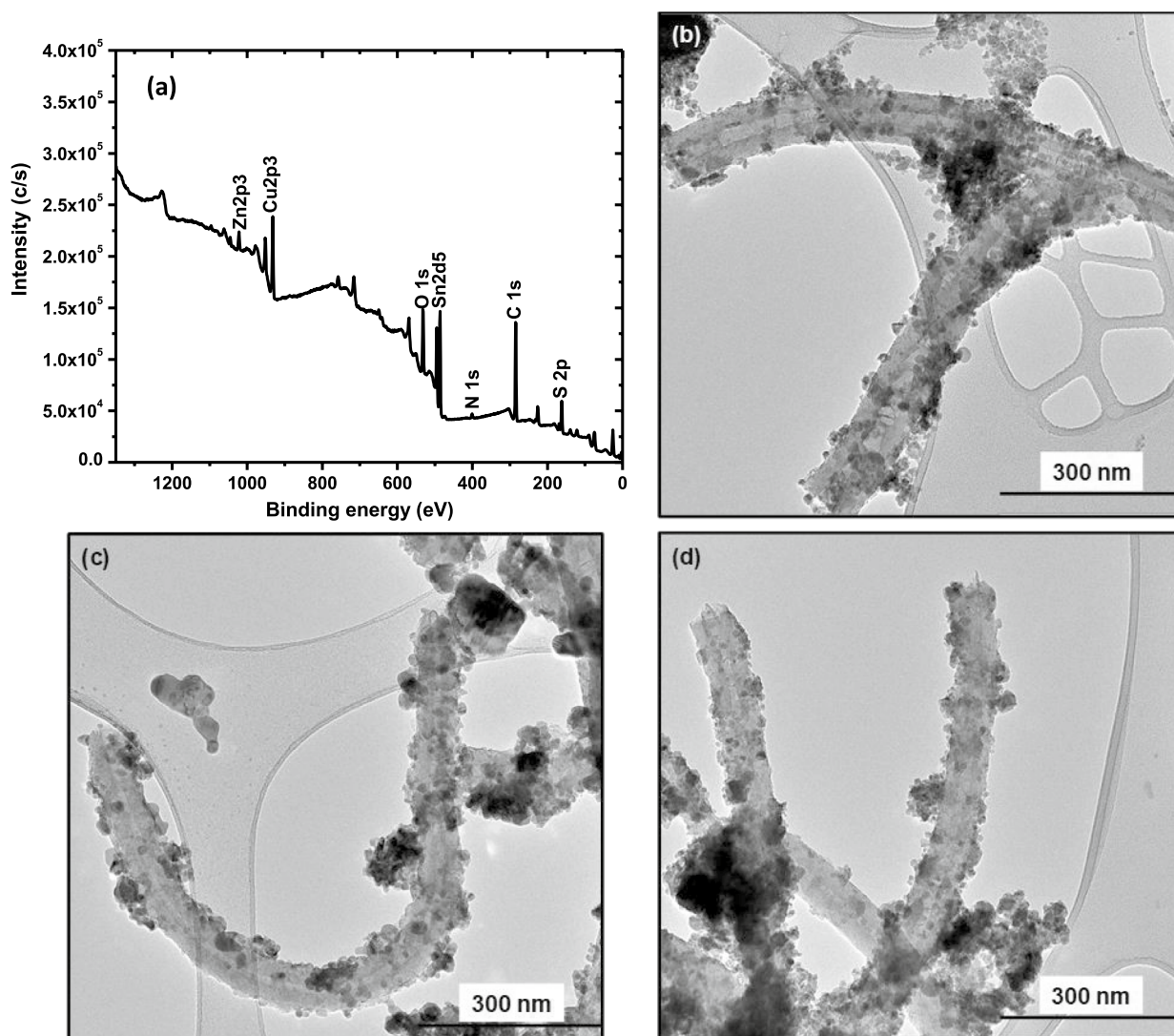


**Figure 2:** (a) XPS survey spectrum of CZTS/N-MWCNTs (0.2). TEM micrographs of CZTS/N-MWCNTs with increasing carbon nanotube mass ratio (b) 0.1, (c) 0.2, and (d) 0.3.

of bamboo compartments within the nanotube structure suggests the incorporation of nitrogen within the graphene layers of the nanotubes [22]. However, the TEM images do not provide clear evidence of whether there is any interaction, either physical or chemical, between the CZTS nanoparticles and the N-MWCNTs.

To confirm the presence of both CZTS and N-MWCNTs in the prepared composites, XPS analysis was conducted. Figures 2(a) and 3 show the XPS survey spectrum of CZTS/N-MWCNTs(0.2) and high-resolution spectra of copper, zinc, tin, sulfur, oxygen, carbon, and nitrogen, respectively. In the XPS survey scan, all atoms present in the constituent materials of the composite are detected, providing solid evidence of successful hybrid formation. Specifically, the Cu, Zn, Sn, and sulfur atoms originate from CZTS, while carbon and nitrogen are found in both CZTS and N-MWCNTs samples.

N-MWCNTs are composed of rolled-up graphene sheets with  $sp^2$ -hybridized carbons and nitrogen atoms, as evidenced by the bamboo-like structure observed in the TEM images of the nanotubes. On the other hand, CZTS is stabilized by an organic ligand, oleylamine, which binds to the CZTS core through its nitrogen head group, as confirmed by proton NMR analysis of both pure oleylamine and OLA-capped CZTS. These organic structures account for the carbon detected in the XPS survey spectrum of the composite. The high-resolution spectra in Fig. 3(a)–(d) further confirm the presence of CZTS. The O 1s and C 1s core-level spectra reveal the oxidation of the surface ligand and the presence of N-MWCNTs. Additionally, a small M–O peak is detected, indicating metal oxidation, which aligns with the XRD results.

The light scattering properties of CZTS, N-MWCNTs, and CZTS/N-MWCNTs hybrids were assessed through diffused reflectance measurements of the powdered samples [Fig. 4]. It was observed that all materials exhibited low reflectance, below 10%, indicating poor light scattering ability. However, this characteristic is not critical for DSSC counter electrode (CE) materials, as the photoanode is primarily responsible for light absorption and should possess good light scattering properties. Among the materials tested, CZTS and CZTS/N-MWCNTs(0.3) exhibited the lowest reflectance, while CZTS/N-MWCNTs(0.1) and CZTS/N-MWCNTs(0.2) showed higher reflectance. Notably, the slightly higher reflectance of CZTS/N-MWCNTs(0.2) suggests that DSSCs employing this CE may have improved light-trapping capabilities [23].

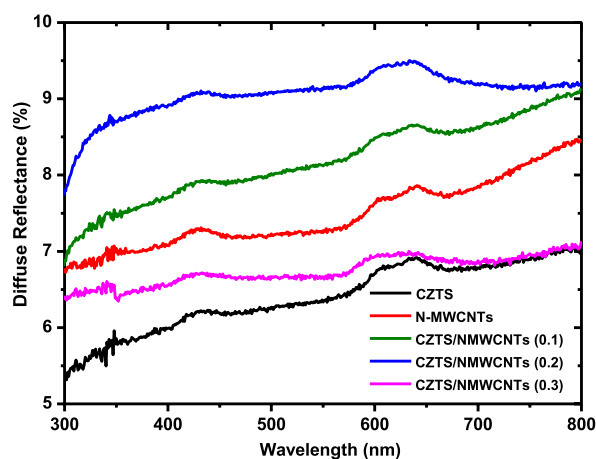


Figure 4: Diffuse reflectance spectra of CZTS, N-MWCNTs, and CZTS/N-MWCNTs composites.

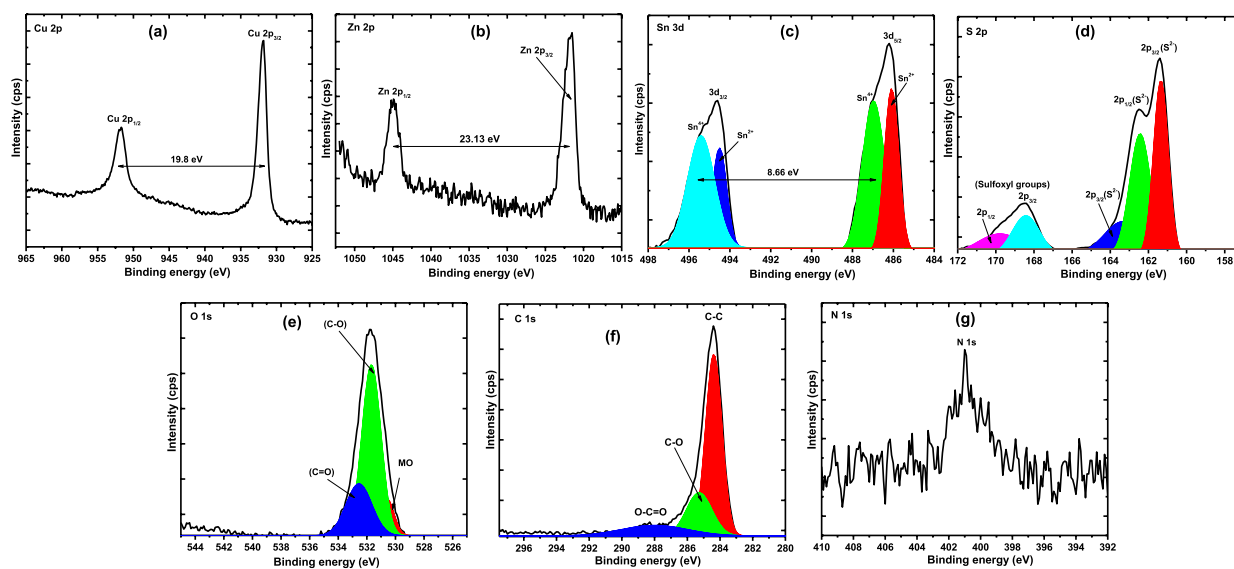
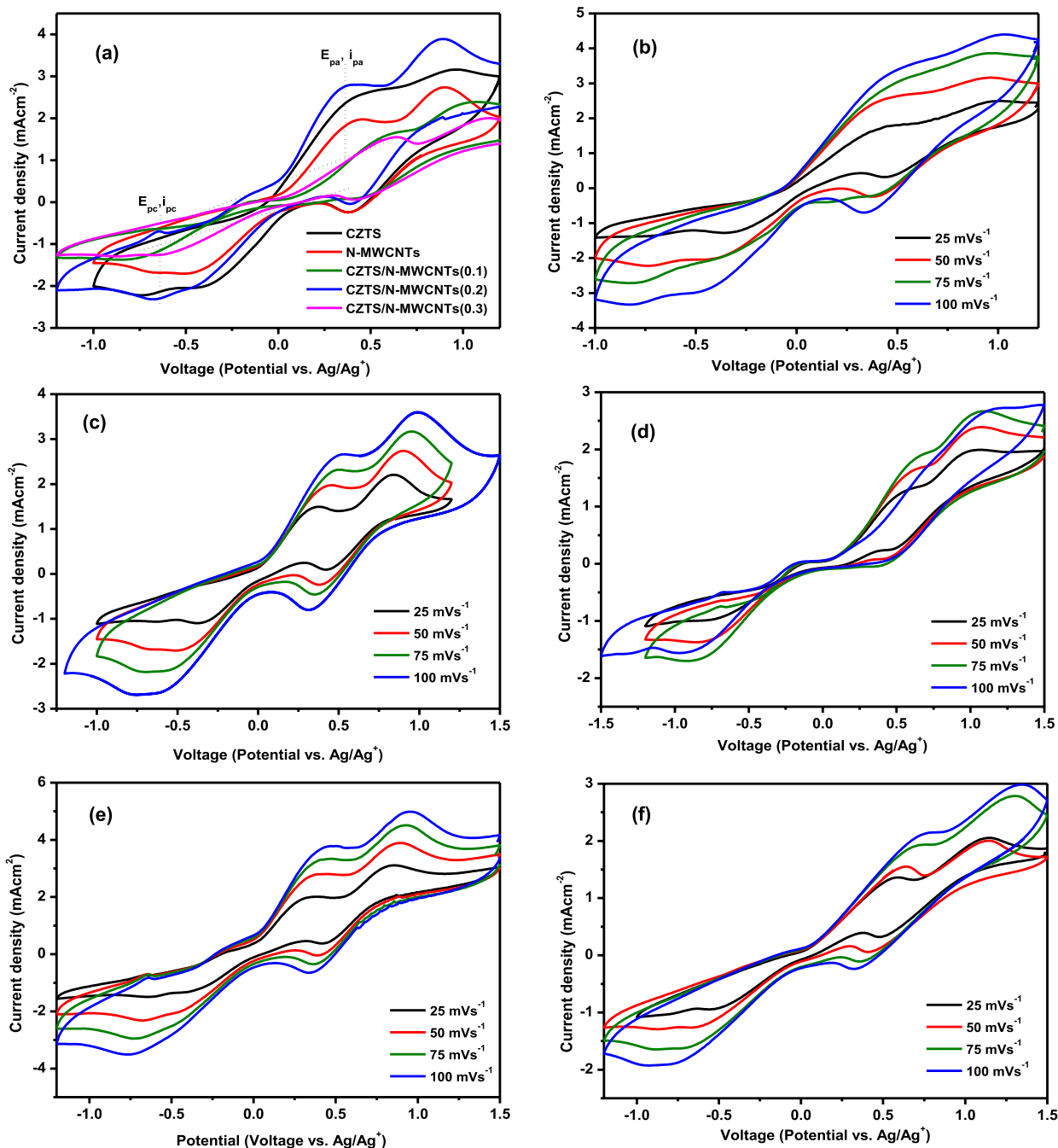


Figure 3: XPS high-resolution spectra of (a) Cu, (b) Zn, (c) Sn, (d) S, (e) O, (f) C, and (g) N in CZTS/N-MWCNTs.

Cyclic voltammetry (CV) was conducted at a scan rate of  $50 \text{ mVs}^{-1}$  to assess the electrocatalytic properties of the counter electrode (CE) materials. Figure 5(a) displays the anodic and cathodic reactions associated with iodide ( $I^-$ ) oxidation and triiodide ( $I_3^-$ ) reduction, respectively. Peak analysis of the CV was performed using EC-Lab software, and the results, including peak–peak separation ( $\Delta E_{pp}$ ) and reduction peak current density, are presented in Table 1. The reduction peak current density

**TABLE 1:** CE electrochemical performance parameters obtained from a three-electrode half-cell setup.

CE	$J_{pc}$ ( $\text{mAcm}^{-2}$ )	$\Delta E_{pp}$ (V)	$\Delta J_{pc}$ ( $\text{mAcm}^{-2}$ )
CZTS	1.267	0.887	0.629
N-MWCNTs	1.012	0.846	0.178
CZTS/N-MWCNTs(0.1)	0.905	1.406	0.259
CZTS/N-MWCNTs(0.2)	1.289	0.967	0.321
CZTS/N-MWCNTs(0.3)	0.517	1.212	0.088



**Figure 5:** (a) Comparison of CV scans of the prepared CE materials at  $50 \text{ mVs}^{-1}$ , cyclic voltammograms of (b) CZTS, (c) N-MWCNTs, (d) CZTS/N-MWCNTs (0.1), (e) CZTS/N-MWCNTs(0.2), and (f) CZTS/N-MWCNTs(0.3) at increasing scan rates.

is highest for CZTS/N-MWCNTs(0.2) at  $1.289 \text{ mAcm}^{-2}$ , followed by CZTS with a value of  $1.267 \text{ mAcm}^{-2}$ , while CZTS/N-MWCNTs(0.3) exhibits the lowest current density at  $0.517 \text{ mAcm}^{-2}$ . This observation aligns with the findings of Tong and colleagues, indicating that CZTS possesses reduction activity and, relative to N-MWCNTs, exhibits a faster reduction reaction rate. Therefore, CZTS can be applied as a CE material in dye-sensitized solar cells [24, 25]. Notably, an increase in the N-MWCNT content to 30 wt % in the composite leads to a CE material with poor catalytic effects on the  $I^-/I_3^-$  electrolyte. This may result from the excessive population of CZTS by nanotubes, leading to the clogging of CZTS's catalytic sites. However, at 20 wt % N-MWCNTs and 80 wt % CZTS, we observe a significant improvement in the catalytic activity of N-MWCNTs and a slight increase in that of CZTS. Nevertheless, the 'duck-line' shape of the CV spectrum is more pronounced for the CZTS/N-MWCNTs(0.2) composite compared to pure CZTS.

The  $\Delta E_{pp}$  (peak–peak separation) follows the following trend: N-MWCNTs < CZTS < CZTS/N-MWCNTs(0.2) < CZTS/N-MWCNTs(0.3) < CZTS/N-MWCNTs(0.1). Both CZTS and N-MWCNTs exhibit low  $\Delta E_{pp}$  values. Notably, at 20 wt % N-MWCNTs, the  $\Delta E_{pp}$  is slightly larger than that of the individual constituent elements. This suggests that CZTS/N-MWCNTs(0.1) requires more energy for facilitating the electrolyte reduction process. Although CZTS exhibits a higher current density and a lower potential, using CZTS/N-MWCNTs(0.2) as the DSSC counter electrode offers the advantage of a more reversible reaction without compromising the activity of CZTS. Figure 5(b)–(f) depict the change in anodic and cathodic peak current densities of the  $I^-/I_3^-$  electrolyte with the square root of the scan rate. In an electron transfer reaction on an electrode surface, the active species undergoes mass transfer, adsorption, and desorption steps. A diffusion-controlled reaction implies that electron transfer depends on mass transfer (movement of ions in solution), and the current density is expected to be directly proportional to the square root of the scan rate. The graphs for all the composites demonstrate a linear relationship between current density at both the anode and cathode electrodes and the square root of the scan rate. This linearity is evident from the plots with  $R^2$  values approximately equal to 1 [Fig. 6], indicating that the oxidation and reduction reactions depend on the diffusion of the electrolyte ion pair in the solution [25–27].

Desirable properties of a good counter electrode (CE) material in dye-sensitized solar cells (DSSCs) include excellent chemical stability in the electrolyte, high electrocatalytic activity, low overpotential, and cost-effectiveness [28]. To assess the stability of the prepared CE materials in the  $I^-/I_3^-$  electrolyte, cyclic voltammetry (CV) tests were conducted. Typically, numerous CV cycles are run at a selected scan rate [29]. Figure 7 illustrates the stability evaluation of the composites

after 50 scan cycles at a scan rate of  $100 \text{ mV/s}$ . The changes in reduction peak current density after 50 cycles are presented in Table 1. The stability ranking of the CE materials is as follows: CZTS/N-MWCNTs(0.3) > N-MWCNTs > CZTS/N-MWCNTs(0.1) > CZTS/N-MWCNTs(0.2) > CZTS. CZTS exhibits the lowest stability. Despite its high catalytic activity toward  $I^-/I_3^-$ , CZTS alone displays poor recyclability and is not a preferred choice for a DSSC CE. However, increasing the concentration of N-MWCNTs in the composites from 10 to 30% enhances the stability of CZTS. It is assumed that at 30%, a significant portion of the CZTS nanoparticles is supported on the walls of the nanotubes.

In a DSSC, the CE plays a crucial role in extracting electrons from the photoanode through an external circuit and facilitating the reduction of  $I_3^-$  ions ( $I_3^- + 2e^- \leftrightarrow I^-$ ). Therefore, the CE material should offer low resistance to electron transfer, both from the external circuit and to the electrolyte. The charge transfer resistance at the CE/electrolyte interface was investigated using electrochemical impedance spectroscopy (EIS) spectra in the  $I^-/I_3^-$  electrolyte, employing a symmetrical cell configuration (CE|electrolyte|CE). The obtained spectra exhibit an arc at high frequency and a semi-circle at low frequency [Fig. 8(a)], and the equivalent circuit is depicted in Fig. 8(c). Notably, the lowest charge transfer resistance ( $R_{ct}$ ) value was observed for N-MWCNTs, which aligns with expectations due to the excellent electron transport properties of carbon nanotubes. For CZTS, an  $R_{ct}$  of  $45 \Omega$  was recorded, which is three times higher than reported by Ngubeni et al. and twice as high as that obtained by Chen et al. [10, 30]. This high  $R_{ct}$  value can be attributed to the semiconductor nature of CZTS, which limits its suitability as an electrode material. However, the incorporation of 10% and 20% N-MWCNTs into CZTS does not improve the  $R_{ct}$  of CZTS; instead, it results in a higher  $R_{ct}$  value. A significant enhancement in the  $R_{ct}$  of CZTS, decreasing from 45 to  $12 \Omega$ , is observed when 30% N-MWCNTs are incorporated into the composite CZTS/N-MWCNTs(0.3). It is evident that a higher loading of nanotubes leads to improved electron transport properties of the semiconductor.

To assess catalytic activity and determine the best-performing counter electrode (CE) material, Tafel polarization curves were obtained from the symmetrical cell in the  $I^-/I_3^-$  electrolyte [Fig. 8(b)]. Tafel plots illustrate the change in  $\text{Log} J$  with potential and provide two essential parameters: the exchange current density ( $J_0$ ) and the limiting current density ( $J_{lim}$ ).  $J_{lim}$  is estimated from the Tafel curve at high potential, while  $J_0$  is determined from the current density value at the intersection of the linear regions of the anodic and cathodic sections of the curve when the potential is zero [31].  $J_0$  is inversely proportional to charge transfer resistance ( $R_{ct}$ ) and is related by Eq. 1. A high  $J_0$  indicates a low  $R_{ct}$ , signifying good electrocatalytic activity of the CE material. Table 2 confirms the relationship between  $R_{ct}$  and  $J_0$ ; CE materials with high  $R_{ct}$

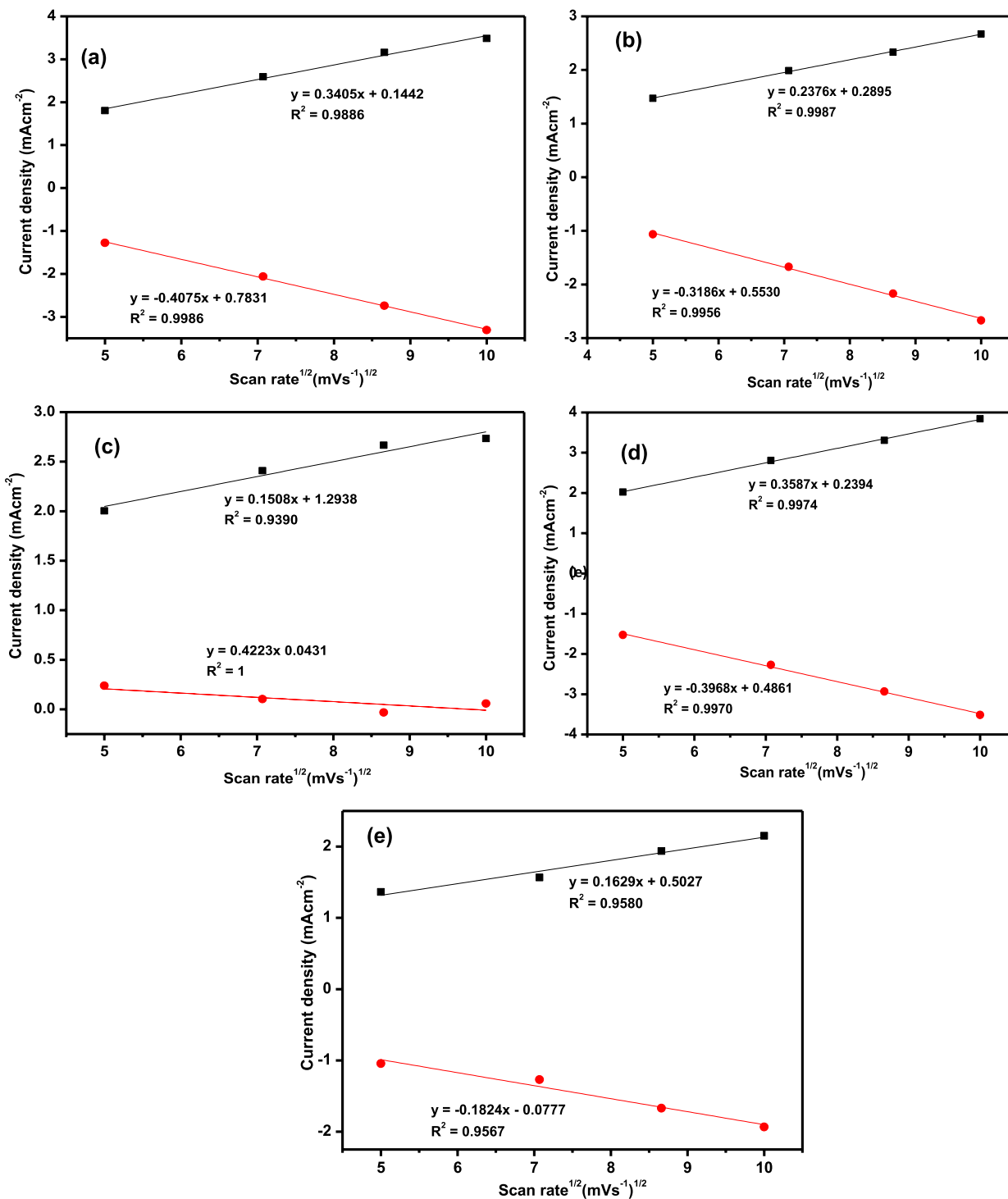


**Figure 6:** Square root of current density plot against oxidation (black) and reduction (black) current density of the prepared composite materials for (a) CZTS, (b) N-MWCNTs, (c) CZTS/N-MWCNTs (0.1), (d) CZTS/N-MWCNTs (0.2), and (e) CZTS/N-MWCNTs (0.3).

values exhibit low  $J_0$  values. Therefore, among the three composite materials, CZTS/N-MWCNTs(0.3) demonstrates higher electro-catalytic activity.

$$J_0 = \frac{RT}{nFR_{ct}} \quad (1)$$

where  $R$  is the gas constant,  $T$  is the temperature (298 K),  $F$  is Faraday's constant,  $n$  ( $n = 2$ ) is the number of electrons, and  $R_{ct}$  is the charge transfer resistance.

Equation 2 relates  $J_{lim}$  to diffusion coefficient,  $D$ .  $J_{lim}$  is the maximum current density that can be passed through the

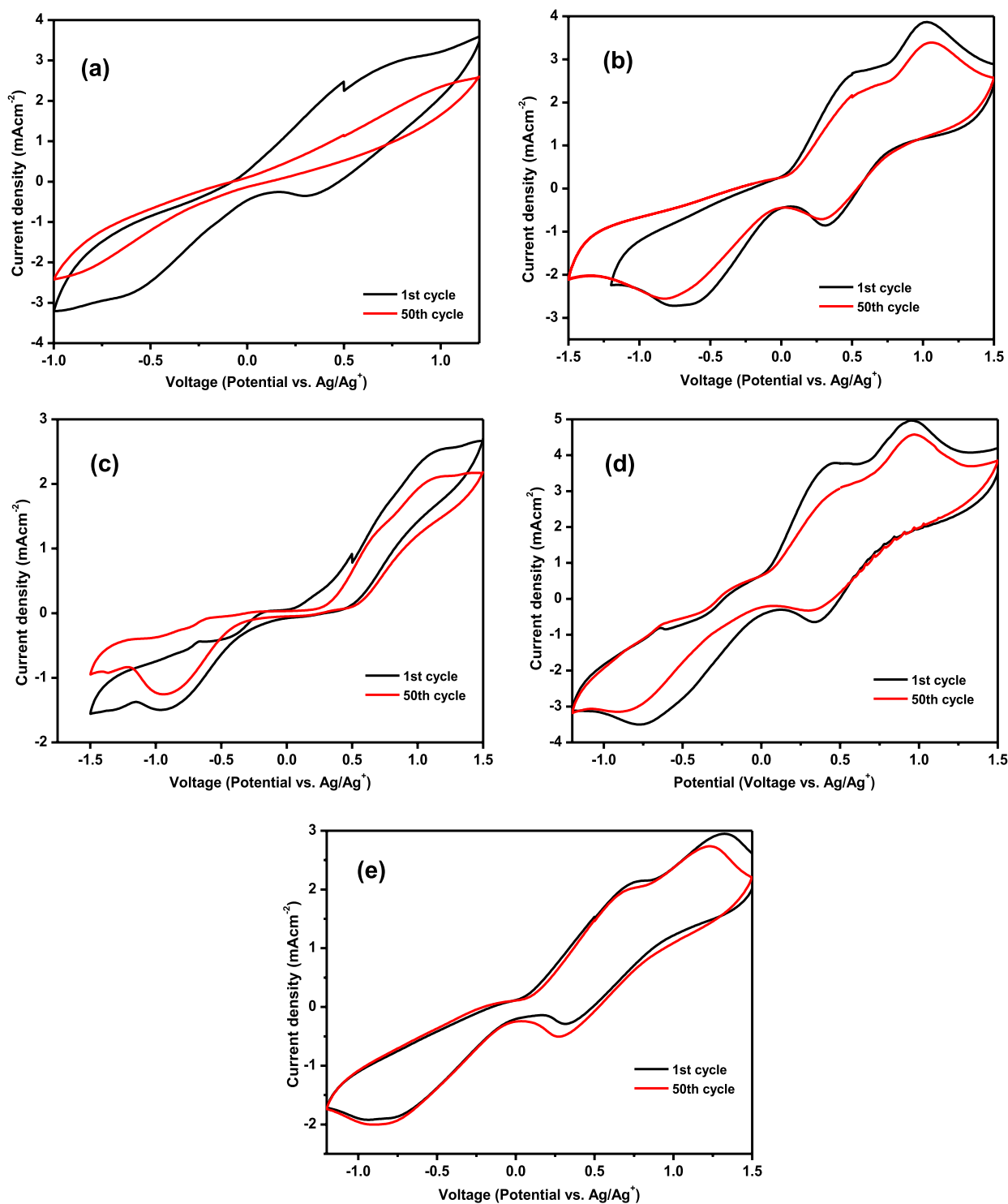


**Figure 7:** Stability evaluation (a) CZTS, (b) N-MWCNTs, (c) CZTS/N-MWCNTs(0.1), (d) CZTS/N-MWCNTs(0.2), and (e) CZTS/N-MWCNTs(0.3) in iodide/triiodide-based electrolyte after 50 cycles at 100 mV/s.

electrolyte [32]. CZTS has the highest value of  $J_{lim}$ , suggesting a high diffusion coefficient when CZTS is employed in DSSC electrolyte, which in turn shows a more electrocatalytic material [28].

$$J_{lim} = \frac{2nFDC}{l} \quad (2)$$

where  $D$  is the diffusion coefficient of the  $I_3^-$ ,  $l$  is the electrolyte thickness,  $n$  is the number of electrons involved in the reduction of  $I_3^-$  at the counter electrode,  $F$  is the Faraday constant, and  $C$  is the iodic concentration.



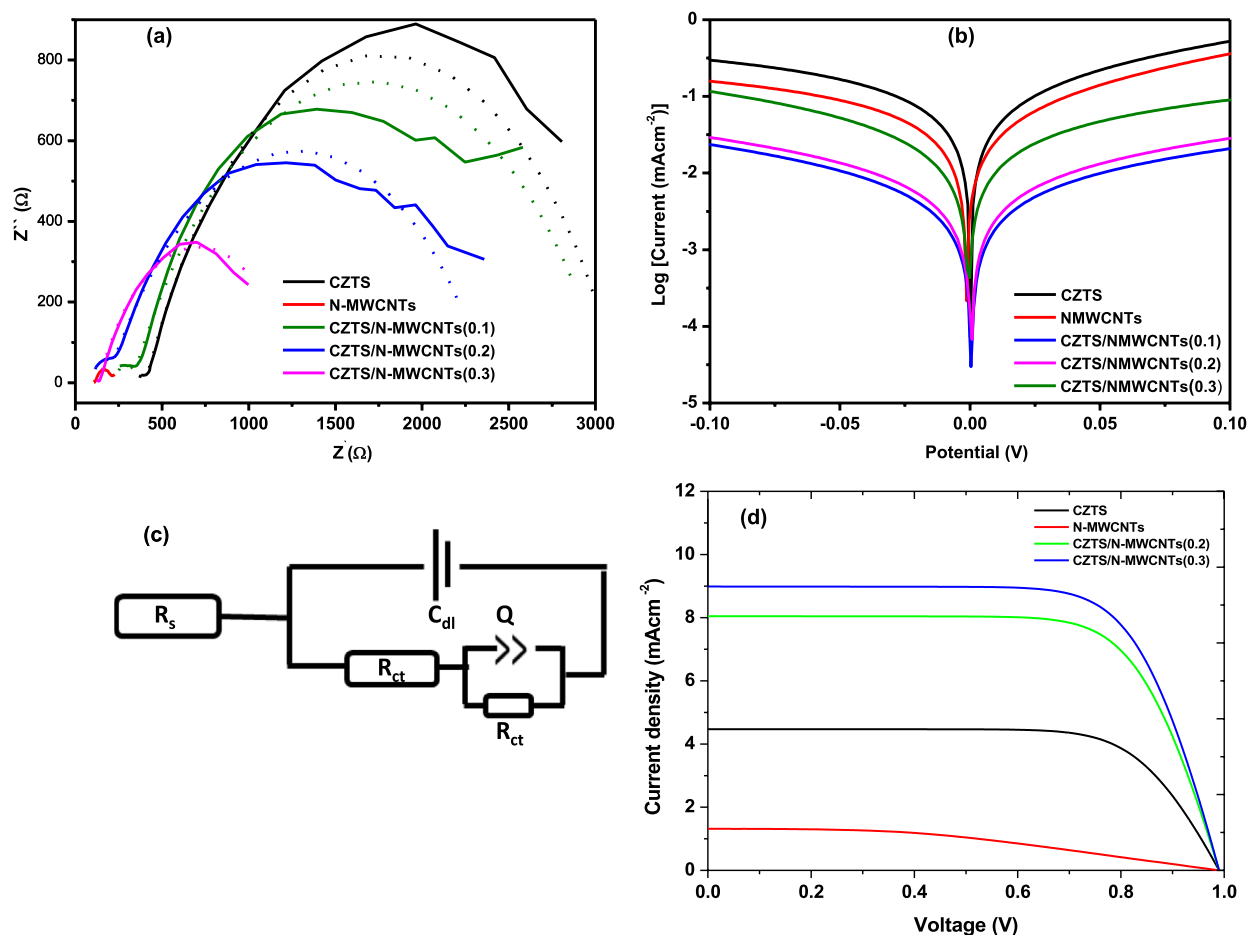


**Figure 8:** (a) Nyquist and (b) Tafel for the  $I^-/I_3^-$  symmetrical cells based on CZTS, N-MWCNTs and CZTS/N-MWCNTs composites, (c) equivalent circuit for the symmetrical cells, and (d)  $J$ - $V$  curves of DSSCs using CZTS, N-WCNTs and CZTS/N-MWCNTs composites.

**TABLE 2:** Electrochemical performance parameters of CE materials obtained from symmetrical cells and  $J$ - $V$  parameters obtained from DSSCs fabricated using the CE materials.

CE	$R_s/\Omega$	$R_{ct}/\Omega$	$J_o/(mAcm^{-2})$	$J_{lim}/(\mu Acm^{-2})$	$J_{sc}/(mAcm^{-2})$	$V_{oc}/V$	FF/%	$\eta/\%$
CZTS	221	45.2	0.106	0.293	4.51	0.99	67	3.0
N-MWCNTs	108	3.8	0.443	0.160	1.31	0.99	40	0.52
CZTS/N-MWCNTs (0.1)	242	92.1	0.035	0.118	-	-	-	-
CZTS/N-MWCNTs (0.2)	105	101.3	0.076	0.029	8.04	0.98	71	5.58
CZTS/N-MWCNTs (0.3)	127	12.57	0.397	0.023	9.03	0.99	73	6.52

The CZTS/N-MWCNTs nanocomposites are deposited on a glassy carbon substrate and immersed in an electrolyte solution ( $I^-/I_3^-$ ). During cyclic voltammetry, electrons traverse through the glassy carbon and the nanocomposite. At the interface between the electrolyte and the composite material, electrons facilitate the reduction of  $I_3^-$  to  $I^-$ . In this process, CZTS catalyzes the reduction reaction, while N-MWCNTs provide high conductivity [33, 34]. Three potential electron transport pathways within the nanocomposite can be proposed. First, electrons may travel from the contact surface to the catalytic sites on CZTS, where the reduction reaction takes place. However,

this route is relatively slow due to the semiconductor nature of CZTS. Second, electrons can move through the CZTS nanoparticles and laterally through the nanotubes. Lastly, electrons can be conducted through the core of the nanotubes to reach the CZTS. The latter two processes occur more rapidly because nanotubes exhibit superior electron conductivity. Additionally, nitrogen doping of the nanotubes, which introduces defects, may further enhance electron mobility through the tubes as they navigate these defects. As a result, CZTS/N-MWCNTs composite CE demonstrates a higher current density compared to the CEs composed of CZTS and N-MWCNTs.

Based on the current density, stability,  $J_0$ , and  $R_{ct}$  results, only CZTS, CZTS/N-MWCNTs(0.2), and CZTS/N-MWCNTs(0.3) CE were integrated into DSSCs. Figure 8(e) illustrates the photocurrent density–voltage curves ( $J-V$  curves) of the DSSCs featuring CZTS, N-MWCNTs, CZTS/N-MWCNTs(0.2), and CZTS/N-MWCNTs(0.3) composite counter electrodes under simulated solar illumination of  $100 \text{ mWcm}^{-2}$  (AM 1.5). From the  $J-V$  curves, key parameters of the DSSCs, including short-circuit current ( $J_{sc}$ ), open-circuit voltage ( $V_{oc}$ ), power conversion efficiency ( $\eta$ ), and fill factor (FF), were obtained and are summarized in Table 2. The  $V_{oc}$  values are relatively consistent across all devices and have a negligible impact on the catalytic performance of the device, as they depend on electron injection efficiency and charge recombination. In contrast, the  $J_{sc}$  values exhibit the following trend: CZTS/N-MWCNTs(0.3) > CZTS/N-MWCNTs(0.2) > CZTS > N-MWCNTs. The same trend is observed for power conversion efficiency (PCE). CZTS/N-MWCNTs(0.3) demonstrates synergistic properties, resulting in improved efficiency.

## Conclusions

The successful synthesis of CZTS/N-MWCNTs nanocomposites was confirmed through XRD, TEM, Raman, and XPS spectroscopies. In this study, the incorporation of N-MWCNTs into the CZTS matrix aimed to enhance the surface area and electron transport properties of CZTS. Among the tested compositions, the CZTS/N-MWCNTs(0.2) sample with 80 wt % CZTS and 20 wt % N-MWCNTs exhibited a high electrochemical current density. Notably, CZTS/N-MWCNTs(0.3) demonstrated superior stability, low exchange current density, and low charge transfer resistance, indicating its relatively higher electrocatalytic activity compared to other materials, including the 20 wt % sample. These findings are consistent with the results obtained from dye-sensitized solar cells (DSSCs), where the CZTS/N-MWCNTs(0.3) device exhibited the highest power conversion efficiency (PCE) of 6.52%.

## Materials and methods

### Chemicals

The following chemicals were purchased from Sigma-Aldrich and used as received; oleylamine (OLA) ( $\text{C}_{18}\text{H}_{37}\text{N}$ , 70%), stannic chloride ( $\text{SnCl}_4 \cdot 5\text{H}_2\text{O}$ , 98%), zinc chloride ( $\text{ZnCl}_2$ ,  $\geq 98\%$ ), copper (I) chloride ( $\text{CuCl}$ ,  $\geq 98\%$ ), elemental sulfur (S, 99.0%), chloroform ( $\text{CHCl}_3$ , 99%), absolute ethanol ( $\text{CH}_3\text{CH}_2\text{OH}$ , 96%), acetonitrile ( $\text{C}_2\text{H}_3\text{N}$ ,  $\geq 99.9\%$ ), lithium iodide (LiI, 99.9%), lithium perchlorate ( $\text{LiClO}_4$ ,  $\geq 95.0\%$ ), iodine ( $\text{I}_2$ ,  $\geq 99\%$ ), *N,N*-dimethyl formamide (DMF) ( $\text{C}_3\text{H}_7\text{NO}$ ,  $\geq 99.5\%$ ), nafion (5 wt %), anhydrous ethylene glycol ( $\text{C}_2\text{H}_6\text{O}_2$ , 99.8%), N719 ruthenium dye (95%), 4-*tert*-butylpyridine ( $\text{C}_9\text{H}_{13}\text{N}$ , 98%), Titania

paste ( $\text{TiO}_2$ , 20 wt %), Whatman glass microfiber filter paper, and Fluorine-doped tin oxide (FTO) glass.

### Colloidal synthesis of $\text{Cu}_2\text{ZnSnS}_4$

The synthesis of CZTS followed the same method as Ngubeni et al. [10], 24 mL of OLA in a three-neck round bottom flask connected to a Schlenk line was heated and refluxed to  $100^\circ\text{C}$  [10]. Then,  $\text{CuCl}$ ,  $\text{ZnCl}_2$  and  $\text{SnCl}_4 \cdot 5\text{H}_2\text{O}$  were sequentially added. The temperature was then increased to  $220^\circ\text{C}$ , upon which elemental sulfur was added. The molar ratio of the precursors added was 2:1:1:4. The color of the solution changed from clear to green upon addition of copper and zinc salts to orange after addition of tin chloride to a black as sulfur was added. The reaction was run for 45 min after which the solution temperature was lowered to  $60^\circ\text{C}$ , and ethanol added to precipitate the colloidal particles out. The nanoparticles were then isolated by centrifugation for three cycles while washing with ethanol, and then dried at room temperature.

### N-MWCNTs preparation by chemical vapor deposition method

The preparation of N-MWCNTs involved two steps. Firstly, the bimetallic Fe–Co catalyst supported on  $\text{CaCO}_3$  (Fe–Co/ $\text{CaCO}_3$ ) was prepared using a known method [22]. Thereafter, 0.3 g of the prepared catalyst was spread on a quartz boat, which was then placed in the middle of a tubular quartz reactor in a horizontal furnace. Nitrogen (40 mL/min) was initially passed through the reactor for 1 h to remove any oxygen within the reactor while increasing temperature of the furnace to  $800^\circ\text{C}$ . Then,  $\text{C}_2\text{H}_2$  and  $\text{N}_2$  gases were bubbled through  $\text{CH}_3\text{CN}$  concurrently at 100 mL/min and 240 mL/min, respectively, for 1 h.  $\text{CH}_3\text{CN}$  was used as both a carbon and nitrogen sources, while  $\text{C}_2\text{H}_2$  was the carbon source and  $\text{N}_2$  transporting medium. Thereafter, bubbling of the respective gases through  $\text{CH}_3\text{CN}$  was terminated and the reactor cooled under flowing nitrogen at 40 mL/min. The prepared carbon compound was weighted, and then acid treated with 3:1 98%  $\text{H}_2\text{SO}_4$ /55%  $\text{HNO}_3$  to remove the catalyst, while oxidizing the terminal carbon atoms, filtered, and washed with distilled water. The acid functionalized sample was named N-MWCNTs.

### Preparation of $\text{Cu}_2\text{ZnSnS}_4$ /N-MWCNTs nanocomposites by agitation

A sonication procedure in DMF for nanocomposite preparation was adapted from Das S. and co-workers [35, 36]. The CZTS samples obtained, and acid-treated N-MWCNTs denoted N-MWCNTs, were used for the preparation of nanocomposites. In a typical reaction, CZTS/N-MWCNTs (10 wt %) (denoted as CZTS/N-MWCNTs(0.10)) was prepared by from 90 mg of CZTS and 10 mg of N-MWCNTs. The composite precursors

were each sonicated in 4 mL of DMF at 40 °C for 1 h. The composite precursor solutions were then mixed and sonicated further for 1 h at the same temperature. Thereafter, the composite material was isolated by centrifuging for three cycles while washing with ethanol, air dried, and ground to a fine powder. Composite materials with 20 and 30 wt % of N-MWCNTs (denoted as CZTS/N-MWCNTs(0.2) and CZTS/N-MWCNTs(0.3), respectively) in CZTS/N-MWCNTs were prepared in a similar manner.

## Electrode fabrication

### Counter-electrode fabrication

Fluorine-doped tin oxide (FTO,  $7 \Omega/\text{cm}^2$ ) cut into 1 by 1 cm pieces was washed by ultrasonication in soap and rinsed with ultra-pure water, followed by further rinsing with acetone and isopropanol. Prior to use, FTO glass was dried with an air gun. The CE inks were prepared by dissolving 40 mg of CZTS, N-MWCNTs and CZTS/N-MWCNTs hybrid materials in 1 mL of ethanol and isopropanol mixture (1:4 v/v) and 25  $\mu\text{L}$  of Nafion, which acts as a binder. 20  $\mu\text{L}$  of the inks was drop casted on FTO glass and heated to 100 °C in an oven to facilitate drying. The CEs were then used as working electrodes in the three-electrode half-cell setup to study their catalytic activity and stability by cyclic voltammetry. The CEs prepared in the same way were then used in the dummy cell to determine the charge transfer resistance as well as the exchange current density by impedance spectroscopy and linear sweep voltammetry, respectively, using the  $\text{I}^-/\text{I}_3^-$  electrolyte. The electrolyte was prepared by dissolving 0.27 g of LiI (0.01 M), 0.1 g of  $\text{I}_2$  (0.001 M), and 2.1 g of  $\text{LiClO}_4$  (0.1 M) in 40 mL of acetonitrile. In cyclic voltammetry, a potential of  $-1.5$  to  $1.5$  V was applied between the working and reference electrodes and current response between the working and counter electrode recorded at increasing scan rates of 25, 50, 75, and 100 mV/s. The stability of the working electrode in the electrolyte was evaluated by running 50 scans at the maximum scan rate of 100 mV/s. For the DSSC device setup, the inks were deposited on  $1 \text{ cm}^2$  of the 1 by 2.5 cm FTO glass.

### Photoanode fabrication

The photoanode was prepared by depositing  $\text{TiO}_2$  paste on  $1 \text{ cm}^2$  area of 1 by 2.5 cm area FTO glass by doctor blade method, then sintered at 350 °C for 30 min in a furnace. The electrode area covered with  $\text{TiO}_2$  was then dipped in a dye sensitizer solution (N719 dye, 0.3 mM in methanol) for 5 times and left to dry at room temperature in a dark place for 24 h.

## DSSC assembly

The DSSC was assembled by sandwiching the sensitized  $\text{TiO}_2$  photoanode electrode and the counter electrode (FTO modified with CZTS, N-MWCNTs, and CZTS/N-MWCNTs), and the electrodes were spaced by a Whatman filter paper. The redox electrolyte (0.05 M iodine, 0.1 M KI, 0.1 M NaI, 0.1 M LiI, 0.5 M 4-*tert*-butylpyridine in acetonitrile) was injected into the filter paper and the device was secured with binder clips. Photocurrent–voltage measurements were then carried out on these devices using HP 4141B source measure unit (SMU) under controlled illumination of  $100 \text{ mW cm}^2$  (AM 1.5 G).

## Characterization

The crystallographic parameters, phase purity of CZTS, and the presence of carbon nanotubes in the CZTS sample matrix were determined by Bruker D2 Phaser Powder X-ray diffractometer using CuK $\alpha$  light source with 2-theta scan from 10 to 90°. The extent of interaction between the CZTS nanoparticles and N-MWCNTs was evaluated by TEM, Raman spectroscopy, and XPS run on FEI Technai T12 TEM microscope, John–Yvon T64000 microRaman spectrophotometer, and Thermo ESCALab 250Xi, respectively. Cyclic voltammetry, linear sweep voltammetry, and impedance spectroscopy measurements were carried out using the Biologic SP 300 potentiostat.

## Acknowledgments

The authors express gratitude to the University of the Witwatersrand (South Africa), the School of Chemistry, and the Microscopy and Microanalysis Unit (MMU) for infrastructural support. This work was funded by both National Research Foundation (NRF) [UID:139214 and 115448] and Department of Science and Innovation-NRF Centre of Excellence in Strong Materials (CoE-SM). Opinions and conclusions arrived at are those of the author and are not necessarily to be attributed to CoE-SM.

## Author contributions

LM (PhD student) and GN (lecturer) contributed to the with materials preparation, data collection and analysis. While the research design, conceptualization and feedback was provided by NM (supervisor) and ZT (supervisor).

## Funding

Open access funding provided by University of the Witwatersrand. This work was supported by the South African National Research Foundation (NRF) [UID: 139214 and

115448] and Department of Science and Innovation-NRF Centre of Excellence in Strong Materials (CoE-SM).

## Data availability

The raw data reported in this study are available from the corresponding author on reasonable request.

## Declarations

**Conflict of interest** The authors have no competing interests to declare that are relevant to the content of this article.

## Supplementary Information

The online version contains supplementary material available at <https://doi.org/10.1557/s43578-023-01260-x>.

## Open Access

This article is licensed under a Creative Commons Attribution 4.0 International License, which permits use, sharing, adaptation, distribution and reproduction in any medium or format, as long as you give appropriate credit to the original author(s) and the source, provide a link to the Creative Commons licence, and indicate if changes were made. The images or other third party material in this article are included in the article's Creative Commons licence, unless indicated otherwise in a credit line to the material. If material is not included in the article's Creative Commons licence and your intended use is not permitted by statutory regulation or exceeds the permitted use, you will need to obtain permission directly from the copyright holder. To view a copy of this licence, visit <http://creativecommons.org/licenses/by/4.0/>.

## References

- M. Ye, X. Wen, M. Wang, J. Iocozzia, N. Zhang, C. Lin, Z. Lin, *Mater. Today* (2015). <https://doi.org/10.1016/j.mattod.2014.09.001>
- R.C. Nelson, *J. Phys. Chem. A* (1965). <https://doi.org/10.1021/j100887a002>
- C. Bhakat, P.P. Singh, *Int. J. Mod. Eng. Res.* **2**, 4 (2012)
- S.C. Mathur, S. Rashidi, W. Wei, *Nanomaterials* (2022). <https://doi.org/10.3390/nano12162761>
- M. Wang, A.M. Anghel, B. Marsan, N.C. Ha, N. Pootrakulchote, S.M. Zakeeruddin, M. Grätzel, *J. Am. Chem. Soc.* (2009). <https://doi.org/10.1021/ja905970y>
- D. Punnoose, H.-J. Kim, C.P. Kumar, S.S. Rao, C.V.V.M. Gopi, S.-H. Chung, *J. Photochem. Photobiol. A* (2015). <https://doi.org/10.1016/j.jphotochem.2015.03.015>
- G. Calogero, P. Calandra, A. Irrera, A. Sinopoli, I. Citro, G.D. Marco, *Energy Environ. Sci.* (2011). <https://doi.org/10.1039/C0EE00463D>
- K.L. Chopra, P.D. Paulson, V. Dutta, *Prog. Photovolt.: Res. Appl.* (2004). <https://doi.org/10.1002/ppp.541>
- S.S. Nemala, K. Mokurala, P. Bhargava, S. Mallick, *Mater. Today: Proc.* (2016). <https://doi.org/10.1016/j.matpr.2016.04.078>
- G.N. Ngubeni, O. Akinbami, L. Mxakaza, S. Nkabinde, T. Kolokoto, F. Otieno, M.J. Moloto, K.P. Mubiayi, N. Moloto, *Thin Solid Films* (2022). <https://doi.org/10.1016/j.tsf.2022.139099>
- X. Sun, J. Dou, F. Xie, Y. Li, M. Wei, *Chem. Commun.* (2014). <https://doi.org/10.1039/C4CC03798G>
- H. Lv, Y. Li, Z. Jia, L. Wang, X. Guo, B. Zhao, R. Zhang, *Compos. B Eng.* (2020). <https://doi.org/10.1016/j.compositesb.2020.108122>
- O. Stephan, P.M. Ajayan, C. Collix, P. Redlich, J.M. Lambert, P. Bernier, *Science* (1994). <https://doi.org/10.1126/science.266.5191.1683>
- V. Stefov, M. Najdoski, G. Bogoeva-Gaceva, A. Buzarovska, *Synth. Met.* (2014). <https://doi.org/10.1016/j.synthmet.2014.09.011>
- J.M. Bell, R.G.S. Goh, E.R. Waclawik, M. Giulianini, N. Motta, *Mater. Forum* **32**, 144–152 (2007)
- G. Yue, J. Wu, J. Lin, Y. Xiao, S. Tai, J. Lin, M. Huang, Z. Lan, *Carbon* (2013). <https://doi.org/10.1016/j.carbon.2012.10.045>
- C.V.V.M. Gopi, S. Ravi, S.S. Rao, A.E. Reddy, H. Kim, *Sci. Rep.* (2017). <https://doi.org/10.1038/srep46519>
- A.J. Haider, M.R. Mohammed, E.A.J. Al-Mulla, D.S. Ahmed, *Rend. Fis. Acc. Lincei* (2014). <https://doi.org/10.1007/s12210-014-0300-6>
- Q. Zhao, H.D. Wagner, *Philos. Trans. R. Soc. A* (2004). <https://doi.org/10.1098/rsta.2004.1447>
- E.T. Thostenson, Z. Ren, T. Chou, *Compos. Sci. Technol.* (2001). [https://doi.org/10.1016/S0266-3538\(01\)00094-X](https://doi.org/10.1016/S0266-3538(01)00094-X)
- K. Kalyanasundaram, J. Kiwi, M. Grätzel, *Helv. Chim. Acta* (1979). <https://doi.org/10.1002/hlca.19780610740>
- Z.N. Tetana, S.D. Mhlanga, G. Bepete, N.J. Coville, S. Afr. J. Chem. **65**, 39–49 (2012)
- N. Santhosh, K.B. Bhojanaa, P. Vijayakumar, M. Senthil Pandian, P. Ramasamy, A. Pandikumar, *J. Mater. Sci. Mater. Electron.* (2020). <https://doi.org/10.1007/s10854-020-02936-4>
- Z. Tong, Z. Su, F. Liu, L. Jiang, Y. Lai, J. Li, Y. Liu, *Mater. Lett.* (2014). <https://doi.org/10.1016/j.matlet.2014.01.136>
- L. Zhu, Y.H. Qiang, Y.L. Zhao, X.Q. Gu, *Appl. Surf. Sci.* (2014). <https://doi.org/10.1016/j.apsusc.2013.11.063>
- X. Zeng, D. Xiong, W. Zhang, L. Ming, Z. Xu, Z. Huang, M. Wang, W. Chen, Y. Cheng, *Nanoscale* (2013). <https://doi.org/10.1039/C3NR01564E>
- E. Mposa, R.K. Sithole, Z. Ndala, G.N. Ngubeni, K.P. Mubiayi, P.M. Shumbula, L.F.E. Machogo-Phao, N. Moloto, *RSC Adv.* (2022). <https://doi.org/10.1039/D2RA00568A>
- G. Yue, F. Li, F. Tan, G. Li, C. Chen, J. Wu, *RSC Adv.* (2014). <https://doi.org/10.1039/C4RA10978C>
- G. Yue, X. Ma, W. Zhang, F. Li, J. Wu, G. Li, *Nanoscale Res. Lett.* (2015). <https://doi.org/10.1186/1556-276x-10-1>
- H. Chen, J. Wang, C. Jia, J. Mou, L. Zhu, *Appl. Surf. Sci.* (2017). <https://doi.org/10.1016/j.apsusc.2017.04.212>

31. S.-H. Chen, J. Tao, H.-J. Tao, Y.-Z. Shen, T. Wang, L. Pan, J. Power. Sources (2016). <https://doi.org/10.1016/j.jpowsour.2016.08.134>
32. Z.J. Hoffman, A.S. Ho, S. Chakraborty, N.P. Balsara, J. Electrochem. Soc. (2022). <https://doi.org/10.1149/1945-7111/ac613b>
33. J.M. Nudent, K.V.S. Santhanam, A. Rubio, P.M. Ajayan, Nano Lett. (2001). <https://doi.org/10.1021/nl005521z>
34. P. Dai, G. Zhang, Y. Chen, H. Jiang, Z. Feng, Z. Lin, J. Zhan, Chem. Commun. (2012). <https://doi.org/10.1039/C2CC17652A>
35. S. Das, K. Sa, I. Alam, P.C. Mahakul, J. Raiguru, B.V.R.S. Subramanyam, P.S. Mahanandia, A.I.P. Conf. Proc. (2018). <https://doi.org/10.1063/1.5035199>
36. S. Das, K. Sa, I. Alam, P. Mahanandia, J. Mater. Sci. (2019). <https://doi.org/10.1007/s10853-019-03467-y>

**Publisher's Note** Springer Nature remains neutral with regard to jurisdictional claims in published maps and institutional affiliations.